Assessment of Metro Manila Urban Parks' Cooling Effect Based on Landscape Metrics Using Threshold Value of Efficiency (TVoE) Approach

Joem C. Guadalupe[1], Jose Daniel G. Gorospe[1], Erica Erin E. Elazegui[1], Jennieveive B. Babaan-Mabaquiao[1]

[1]Department of Geodetic Engineering, University of the Philippines Diliman, Quezon City 1101 Philippines
– (jcguadalupe, jdgorospe, eeelazegui, jbbabaan)@up.edu.ph

Keywords: Urban Heat Island, urban parks, landscape metrics, Park Cooling Effect Indices, piecewise linear regression

Abstract

In highly urbanized and climate-vulnerable cities such as Metro Manila, the Urban Heat Island (UHI) effect intensifies thermal stress. Urban parks can mitigate this by maximizing their cooling effect amidst the space constraints caused by urbanization. This involves the identification of optimal thresholds for spatial characteristics such as size, vegetation-water ratio, shape complexity, fragmentation, aggregation, and patch density to produce actionable values for realistic park design and planning. This study examines how compositional and configurational landscape metrics influence the cooling effects of 25 urban parks in Metro Manila. Land Surface Temperature (LST) was retrieved from Landsat 8 imagery using the split-window algorithm, while land cover was classified using a Random Forest model with 87.5% test accuracy. Landscape metrics were computed using FRAGSTATS, and four Park Cooling Effect Indices were derived: Park Cooling Area (PCA), Park Cooling Intensity (PCI), Park Cooling Efficiency (PCE), and Park Cooling Gradient (PCG). To determine the Threshold Value of Efficiency (TVoE), piecewise linear regression (PLR) was chosen among the regression models as it yielded the most interpretable and statistically valid TVoEs. Results show that vegetation metrics such as PLAND V (percentage landscape), CA V (total area), and ENN_MN (mean Euclidian nearest neighbor distance) significantly influence PCI and PCE, though often with negative relationships, which indicates diminishing returns beyond certain values. Meanwhile, water-based metrics such as PLAND W (percentage landscape) and AI W (aggregation index) showed moderate to strong associations with PCA and PCG, particularly when water patches were aggregated or well-distributed. These findings provide empirical thresholds to inform climate-responsive park planning and offer actionable insights for enhancing thermal resilience in dense urban settings.

1. Introduction

Rapid urbanization and population growth have led to widespread land conversion, replacing natural landscapes with impervious built-up surfaces. These changes increase solar absorption and generate warmer urban areas, hence resulting in the Urban Heat Island (UHI) effect, where cities experience relatively higher land surface and air temperatures than surrounding rural areas (Oke, 1981).

Unlike impervious surfaces, vegetation and water bodies retain less solar radiation due to their higher albedo and cooling processes. Vegetation cools through shading and evapotranspiration, while water moderates temperature through evaporation, convection, and high heat capacity. Together, these features form blue-green spaces (BGS), which synergistically reduce thermal stress within urban areas (Gupta et al., 2019; Yu et al., 2021). Urban parks, a form of BGS, are designated spaces dominated by vegetation and water that deliver environmental, social, and recreational benefits.

These cooling effects of urban parks are typically assessed using four LST-based indices: Park Cooling Area (PCA), Park Cooling Intensity (PCI), Park Cooling Efficiency (PCE), and Park Cooling Gradient (PCG) (Wu et al., 2024). Specifically, PCI measures the magnitude of LST reduction within and around the park, PCE assesses cooling per unit area, PCG reflects the steepness of LST gradients, and PCA delineates the spatial extent of thermal influence. These indices have proven useful in quantifying the cooling benefits of urban parks in regions like China, India, and the Middle East, where impervious urbanization exacerbates thermal stress (Hu et al., 2023).

PCE is closely tied to landscape structure. Compositional metrics describe the proportion and variety of land cover types, while configurational metrics quantify the spatial distribution, shape, and orientation of land cover patches. In landscape ecology, a patch refers to a spatially continuous area of a single land cover type that is distinct from its surroundings; in this study, patches specifically refer to contiguous areas of vegetation and water within BGS (Pang et al., 2022). As urban planners increasingly use landscape metrics, identifying the optimal BGS structures becomes essential for effective climate adaptation (Costanza et al., 2019).
Despite extensive research, there is no consensus on how spatial factors influence park cooling as it varies with context specific conditions such as urban form, climate type, seasonality, and latitude (Pang et al., 2022). To maximize cooling outcomes, recent studies have introduced the Threshold Value of Efficiency (TVoE) framework, which posits that each landscape metric has a critical value beyond which additional increases yield diminishing thermal returns (Fan et al., 2019; Peng et al., 2020). This principle, grounded in the law of diminishing marginal utility, aids urban planners in optimizing land use and resource allocation. Originally modeled using logarithmic regression, TVoE analysis has expanded to include cubic, piecewise linear, and generalized additive models to accommodate urban heterogeneity (Yu et al., 2020).

In Metro Manila, where rapid urbanization intensifies UHI risks, applying the TVoE framework to analyze park cooling effects remains largely unexplored. Given the localized and seasonal nature of park cooling dynamics, this study focuses on how compositional and configurational landscape metrics influence the cooling performance of 25 urban parks in Metro Manila. Specifically, this is done through calculating their landscape

https://doi.org/10.5194/isprs-annals-X-5-W4-2025-285-2026

metrics and park cooling effect indices (PCEIs) and regressing it via PLR to identify the TVoE of the landscape metrics.

2. Data and Methods

This study mainly utilized a single 30-m resolution Landsat 8 OLI/TIRS Level 1 and Level 2 dataset dated March 6, 2024, for LST retrieval and supervised classification, respectively. Water vapor for the split-window algorithm was obtained from MODIS/Terra MOD05_L2 and MYD05_L2 products. Landsat-derived LST was cross-validated using MODIS daily LST product MOD11A1 Version 6.1 for the same date. The Random Forest classifier was trained using the 2020 National Mapping and Resource Information Authority (NAMRIA) LULC dataset. Finally, urban park boundaries were delineated using a dynamic combination of Department of Natural Resources – National Capital Region (DENR-NCR) list of recreational parks and OpenStreetMap boundary shapefiles. Shown below is a flowchart of the study's workflow.

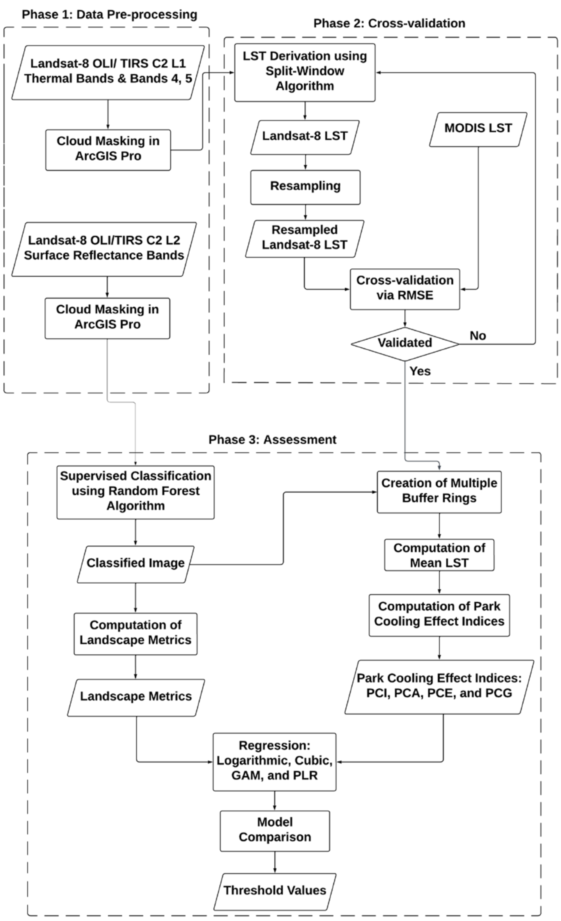

Figure 1. Flowchart of the Study's Workflow

2.1 Study Area

Metro Manila, the Philippines' largest urban center and central business district, ranks among the world's five largest metropolitan areas (Oliveros et al., 2019). Due to rapid urbanization since the 1970s, the region has experienced intensified UHI effects than its neighboring regions, reflected in rising average temperatures and extreme heat indices reaching 38°C–46°C in May 2024 (DOST & PAGASA, 2024). This study focuses on the urban parks of Metro Manila as critical BGS mitigating UHI effects. The original study area was extended slightly beyond the administrative boundary of Metro Manila to ensure methodological completeness. Several urban parks are located at or near the region's edge, restricting the analysis within the administrative limits would have excluded surrounding areas critical for accurately computing LST gradients and the park cooling effect. Including these adjacent buffer zones prevents premature boundary effects and ensures a more accurate spatial analysis of park cooling effects. Shown below is the study area.

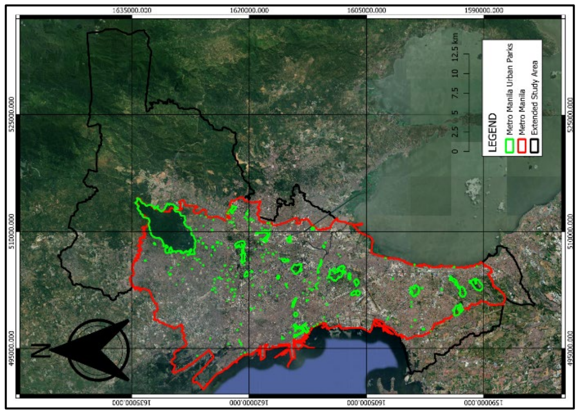

Figure 2. Map showing the original study area (red), extended study area (black), and the urban parks (green)

2.2 LST Retrieval

The split-window algorithm proposed by Jimenez-Muñoz and Sobrino (2008) was used for LST retrieval of a Landsat image acquired on March 6, 2024. This image was selected due to minimal cloud cover and alignment with the dry season; a critical period for assessing the cooling potential of BGS. Such algorithm demonstrated the highest theoretical accuracy among the four types of split-window algorithms validated by Ye et al. (2022). The LST (K) was computed as:

$$\begin{aligned} LST \; &= TB_{10} + C_1(TB_{10} - TB_{11}) + C_2(TB_{10} - TB_{11})^2 \\ &+ C_0 + (C_3 + C_4 W)(1 - m) + (C_5 + C_6 W)\Delta m, \end{aligned} \tag{1}$$

where TB_{10} and TB_{11} = brightness temp. of band 10 and 11
C_0 to C_6 = split-window constants
W = atmospheric water vapor
m = mean land surface emissivity (LSE)
Δm = difference in LSE

Bilinear interpolation was used to resample the Landsat LST to match the 1000 m spatial resolution of MODIS LST. The split-window algorithm (SW10) used in this study was among the ten algorithms evaluated by Arabi Aliabad et al. (2020) for deriving LST from Landsat imagery using a temperature-based method and cross-validation against MODIS LST. In the cross-validation phase, SW10 recorded the lowest RMSE among all the algorithms evaluated, at 3.56°C. This value was adopted as the benchmark for evaluating the accuracy of the Landsat LST. With that, the computed RMSE was 2.622°C, which is well below the reference threshold, hence indicating acceptable accuracy.

2.3 Land Cover

Using Google Earth Engine, a random forest classification model was developed using training points obtained from the 2020 NAMRIA LULC dataset and the Landsat 8 image. The land cover analysis therefore utilized two time points: the 2020 NAMRIA LULC dataset for training and validation, and a single-date Landsat 8 image acquired on March 6, 2024, for classification and analysis. The classifier's performance was assessed by setting an 80% threshold for all accuracy metrics (overall, kappa, user, and producer). After satisfying the accuracies, the model was tested using the 2024 dataset and a classified map of Metro Manila was generated. Pixels classified as built-up were removed as the study only focused on vegetation and water classes.

2.4 Calculation of Landscape Metrics

Type	Metric Name	Interpretation
Compositional	PERIM	PERIM > 0; (m) At patch level, it represents the edge of a pixel.
	CA V	CA > 0; (has) At class level, it is the area of class measured per pixel.
	PLAND	0 < PLAND ≦ 100; (%) quantifies the proportional abundance of each patch type in the landscape.
	PD	PD > 0; (dimensionless) Number of classes present per 100 hectares.
	SHDI	0 < SHDI ≦ 0.693; (dimensionless) Closer to 0, a certain class dominates. Closer to 0.693, equally distributed.
Configurational	SHAPE_ MN	SHAPE_MN ≥ 1; (dimensionless) 1 signifies that the shape is square, it increases without limit as shape becomes more irregular.
	AI	0 ≦ AI ≦ 100; (%) Closer to 0 signifies complete fragmentation, otherwise signifies the opposite.
	DIVISIO N	0 ≦ DIVISION ≦ 1; (dimensionless) Closer to 0 signifies lower fragmentation, otherwise the opposite.
	ENN_MN	ENN_MN ≥ 0; (m) d_i is the average distance of one vegetation patch to its nearest neighbor patch of water.

Table 1. Configurational and Compositional Landscape Metrics

FRAGSTATS was used to calculate the landscape metrics of Metro Manila urban parks. Table 1 shows the minimum landscape patterns that comprehensively describe the landscape structure of urban parks proposed and used by previous studies such as Polydoros et al., (2022) and Yan et al., (2024).

2.5 Calculation of Park Cooling Effect Indices

The park cooling distance is the prerequisite for the computation of the PCEIs. The 30 buffer rings at 30-meter intervals and their corresponding mean LST values were used to fit cubic regression models, from which the park cooling distances were computed by determining the local maximum of each curve. In the case of multiple local maxima, the highest LST was selected as it represents the last peak before the LST stabilizes.

PCA was computed by generating buffers corresponding to the cooling distance of each park and computing the enclosed areas. PCI, PCE, and PCG were calculated using the equations below.

$$PCI = LST_{TP} - LST_{Park}, \tag{2}$$

where LST_{TP} = mean LST at the computed cooling distance
LST_{Park} = mean LST of the park itself

$$PCE = \frac{PCA}{S_{park}}, \tag{3}$$

where S_{park} = area of the park

$$PCG = \frac{PCI}{L}, \tag{4}$$

where L = maximum cooling distance.

2.6 Calculation of TVoEs

Four regression models were tested for the calculation of the TVoEs of each landscape metric in relation to the park cooling effect indices: logarithmic, cubic, generalized additive model (GAM), and piecewise linear regression (PLR). Ultimately, PLR provided a data-driven alternative to identifying TVoE through experimentally detected breakpoints as shown in Figure 3. It models the relationship by fitting two linear segments:

$$y = \begin{cases} m_1 x + b_1, & if\ x < x_{BP} \\ m_2 x + b_2, & if\ x \geq x_{BP}, \end{cases} \tag{5}$$

where m_1 and m_2 = slopes before and after the breakpoint
b_1 and b_2 = intercepts before and after the breakpoint
y = PCEI
x = landscape metric
x_{BP} = breakpoint

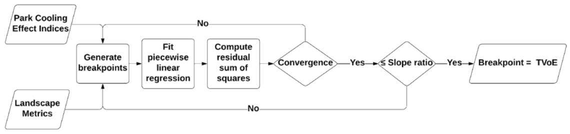

Figure 3. TVoE Computation Process

The breakpoint, interpreted as the TVoE, was calculated using least squares optimization implemented using differential evolution of the piecewise linear fitting (pwlf) Python library. To ensure that the post-TVoE behavior showed diminishing marginal utility, slope ratios were evaluated using a weighted composite scoring based on the number of valid TVoEs (w_1 = 0.5), flatness (w_2 = 0.25), and mean R^2 (w_3 = 0.25). We identified 0.27 was as the optimal slope ratio threshold based on evaluation.

3. Results and Discussion

3.1 LST Retrieval Using Split-window Algorithm

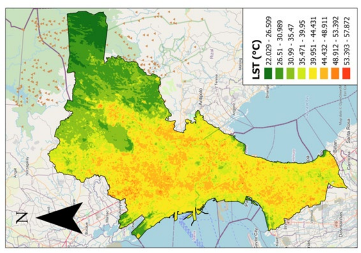

Figure 4. Landsat Derived LST on March 6, 2024

Figure 4 shows that elevated LST values are concentrated in Manila, Makati, Mandaluyong, and Pasay, highlighting persistent thermal hotspots associated with the UHI effect. These patterns confirmed findings that dense built-up areas exhibit higher temperatures due to increased heat retention and low albedo. This reinforces the need to assess the cooling capacity of the Metro Manila urban parks. Conversely, lower LST values are observed in parts of Quezon City, Marikina, and Pasig, suggesting the presence of vegetation or water bodies. Moderate

https://doi.org/10.5194/isprs-annals-X-5-W4-2025-285-2026

temperatures are evident near water systems such as the Pasig River, Marikina River, La Mesa Watershed, Manila Bay, and Laguna Lake. These cooler zones may be attributed to existing riparian buffers and are consistent with literature emphasizing the cooling effect of vegetated and water bodies due to their higher albedo and evapotranspiration. The observed spatial variation in LST thus aligns with expected land cover characteristics.

To ensure spatial alignment prior to cross-validation, Figure 5a shows the Landsat-derived LST that was resampled to match the coarser resolution of MODIS LST using bilinear interpolation.

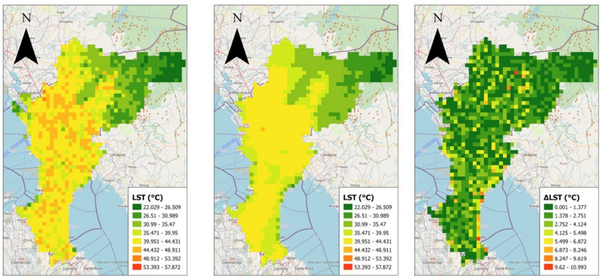

(a) (b) (c)

Figure 5. (a) Resampled Landsat LST using Bilinear Interpolation, (b) MODIS LST, (c) Absolute Error of (a)

Figure 5c shows the absolute error raster to provide an intuitive spatial visualization of pixel-level discrepancies between MODIS and Landsat LST. Using bilinear interpolation, absolute errors ranged consistently from 0.001 °C to 4.124 °C (dark to light green), indicating generally low error magnitudes.

Cross-validation of LST values revealed that bilinear interpolation achieved minimal pixel-level error variation. Specifically, the method resulted in a minimum absolute error of 4.578×10^{-5} °C, a maximum absolute error of 10.458 °C, a mean absolute error of 2.057°C, and a root mean square error (RMSE) of 2.622 °C. These closely clustered values indicate stable error distribution and acceptable performance. Bilinear interpolation thus provided a suitable balance between theoretical soundness and empirical reliability, justifying its use in this study.

3.2 Land Cover

To ensure reliable classification, the Random Forest model was first validated using the 2020 NAMRIA LULC dataset before applying it to single 2024 Landsat-8 imagery on March 6 for a temporal alignment with the LST retrieval. This two-year framework, 2020 for training and validation, and 2024 for classification and analysis, ensured methodological robustness while capturing contemporaneous land cover conditions. Table 2 shows that the model achieved high accuracy (90.6% OA, 0.858 KA), confirming its ability to distinguish vegetation, water, and built-up areas despite class imbalance.

Metric	2020 Train Model		2024 Test Model	
Overall	0.906		0.875	
Kappa	0.858		0.811	
User	Vegetation	0.884	Vegetation	0.858
	Water	0.951	Water	0.951
	Built-up	0.883	Built-up	0.810
Producer	Vegetation	0.940	Vegetation	0.924
	Water	0.885	Water	0.873
	Built-up	0.890	Built-up	0.817

Table 2. Random Forest Model Accuracies.

When applied to 2024 data, accuracy remained strong (87.5% OA, 0.811 KA), with consistent detection of vegetation and water, especially important for this study. While built-up classification slightly declined, the model continued to capture the target classes with sufficient accuracy, justifying the use of the 2024 land cover map in landscape metric calculations. Only vegetation and water classes were retained for further analysis using validated park boundaries. Figure 6 shows the classified image of Metro Manila in year 2024.

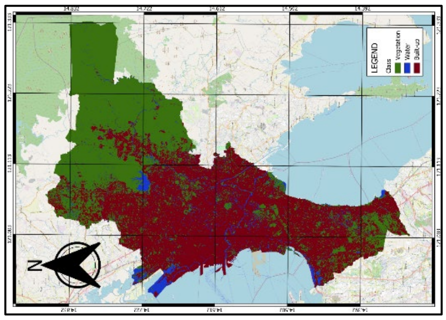

Figure 6. 2024 Classified Image of Extended Study Area.

3.3 Metro Manila Urban Parks' Landscape Metrics

3.3.1 Compositional Metrics: Vegetation class area (CA V) varied significantly, from 0.52 ha in Makati Park to 106.63 ha in Jamboree Park, reflecting differences in park scale. In most cases, water class area (CA W) was smaller, except in parks adjacent to rivers such as Arroceros Forest Park, Fort Santiago, and Luntiang Pilipinas Forest Park. Notably, Marikina River Park presented a balanced composition with PLAND V and PLAND W values at 49.558% and 50.442%, respectively.

Patch density (PD) showed wide variation, ranging from 6.674 to 224.404 for vegetation and from 64.028 to 472.328 for water. These variations suggest the absence of dominant patch structures and point to differing degrees of fragmentation among parks. Shannon's Diversity Index (SHDI) also varied, with Marikina River Park having the most balanced diversity (SHDI = 0.693). Parks with low SHDI, such as Philippine Navy Golf Club (SHDI = 0.119), reflected dominance by a single class.

3.3.2 Configurational Metrics: Shape complexity, measured by SHAPE_MN, was more variable for vegetation (range: 1.123–2.765) than for water (1.062–1.276), indicating greater irregularity in vegetative patch shapes. Aggregation Index (AI) values showed that vegetation patches were generally highly aggregated (AI V > 80%), while water patches exhibited greater variability. Correspondingly, DIVISION V values were low, indicating less fragmentation of vegetation patches, while DIVISION W was more variable.

Connectivity, measured through ENN_MN, ranged from 23.179 m to 54.098 m, with greater distances observed in larger parks such as Philippine Navy Golf Club. This suggests that class connectivity decreases as park area increases due to the spatial separation of blue and green spaces within larger parks.

3.4 Park Cooling Effect Indices

PCA ranged from 31.47 ha to 281.12 ha (mean: 164.32 ha), with higher values generally associated with larger parks. Strong correlations were found between PCA and size-based landscape metrics such as PERIM V (r = 0.739) and CA V (r = 0.685), affirming that inherent park size plays a dominant role in expanding cooling coverage. While cooling distance mathematically contributes to PCA, its influence was comparatively moderate (r = 0.464), as smaller parks with large cooling distances still yielded lower PCA values. Moreover, negative correlations with SHAPE_MN W (r = –0.316) and AI W (r = –0.399) suggest that simpler and less aggregated water patches enhance PCA.

PCI values ranged from 0.68 °C to 8.15 °C (mean: 4.72 °C), indicating that most parks provide a cooling effect of nearly 5 °C compared to their surroundings. The strongest associations were found with water-related metrics, including AI W (r = 0.421), PLAND W (r = 0.368), and ENN_MN (r = 0.410), suggesting that highly aggregated and well-distributed water features contribute significantly to thermal intensity. Conversely, negative correlations with PD W (r = –0.498) and DIVISION W (r = –0.451) imply that fragmented water features reduce PCI. These results align with existing literature on the thermal regulatory role of water bodies via evaporative cooling and thermal inertia. Importantly, PCI is context-sensitive and should be interpreted in conjunction with other indices.

PCE measures cooling effectiveness relative to park size. Values ranged widely, with outliers such as Arroceros Forest Park (18.33), San Juan Reservoir (12.92), and Fort Santiago (10.70) showing cooling spreads many times greater than their area. These high values are consistent with studies from China, where PCE was shown to be enhanced by dense vegetation, irregular shapes, and compact urban surroundings. Strong positive correlations were found with AI W (r = 0.610) and DIVISION V (r = 0.580), indicating that cohesive water features and moderately fragmented vegetation patches contribute to high efficiency. Negative correlations with CA V (r = –0.664) and PLAND V (r = –0.691) reflect that larger vegetative cover does not always translate to higher efficiency. These inverse relationships with PLAND W (r = 0.691) and DIVISION W (r = –0.597) suggest a trade-off between green and blue spaces, underscoring the importance of spatial balance in park design.

PCG captures the LST reduction rate per meter of cooling distance. While values ranged modestly across parks, higher PCG was strongly associated with water-related metrics, notably AI W (r = 0.388), CA W (r = 0.327), and ENN_MN (r = 0.420). This implies that large, aggregated, and spatially dispersed water bodies generate steeper thermal gradients. In contrast, negative correlations with PD W (r = –0.492) and DIVISION W (r = –0.342) suggest that fragmented water patches reduce the rate of temperature drop. These patterns reinforce the central role of water configuration in shaping thermal gradients, in alignment with PCI and PCE dynamics.

3.5 Threshold Values of Efficiency

The Threshold Values of Efficiency (TVoEs) were computed using piecewise linear regression (PLR) by identifying breakpoints in each landscape metric-park cooling effect index (LM–PCEI) regression pair. TVoEs are presented according to their corresponding PCEI such as PCI, PCA, PCE, and PCG, to allow contextualized interpretation. This organization aligns each landscape metric with its relevant urban cooling context, facilitating targeted planning strategies and design objectives.

Figure 7 shows the computed TVoEs and corresponding plots of landscape metrics associated with PCI, which reflects the magnitude of thermal relief provided by parks. PCI is especially relevant in dense, impervious urban areas with high heat stress, where the planning objective is to maximize surrounding thermal relief.

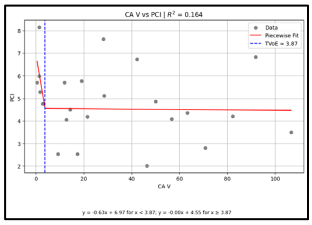

(a) CA V = 3.87 has

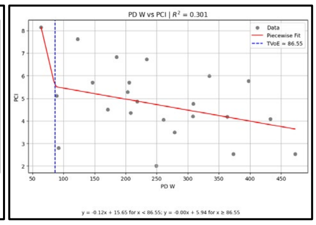

(b) PD W = 86.55

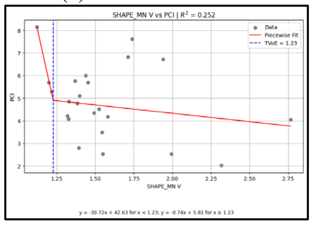

(c) SHAPE_MN V = 1.23

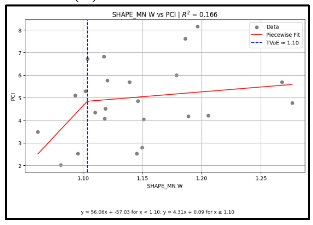

(d) SHAPE_MN W = 1.10

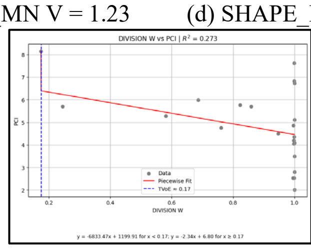

(e) DIVISION W = 0.17

Figure 7. LM – PCI Trend and TVoEs

Among the metrics, SHAPE_MN W exhibited classical diminishing marginal utility with a TVoE of 1.10, indicating that cooling benefits peak when water patches have simpler shapes; further increases yield diminishing returns. In contrast, CA V, PD W, SHAPE_MN V, and DIVISION W demonstrated negative marginal utility, which serves as a basis for tradeoff benchmarks in constrained urban settings.

A TVoE of 3.867 ha for CA V marks the threshold below which PCI declines steeply. For PD W, a TVoE of 86.555 patches per 100 ha suggests minimizing fragmentation, though values above this point are tolerable due to slower PCI decline. Similarly, a TVoE of 1.228 for SHAPE_MN V implies that simpler vegetation shapes are optimal, but deviations are acceptable beyond this point. DIVISION W's TVoE of 0.175 supports aggregated water patches as ideal, while allowing slight fragmentation under practical constraints.

Figure 8 shows the computed TVoEs and corresponding plots of landscape metrics associated with PCA, a cooling metric best prioritized in urban contexts with sufficient space, where expanding the spatial extent of park influence is most effective. AI V, CA W, PERIM V, PERIM W, PLAND W, and SHAPE_MN V all exhibited classical diminishing marginal utility. This indicates that their respective TVoEs mark the point of maximum PCA benefit, beyond which marginal gains decline.

AI V peaked at a TVoE of 77.621, favoring aggregated vegetation. CA W's TVoE of 2.93 ha identifies the optimal cumulative size of water patches. PERIM V and PERIM W reached optimal PCA values at 17,460 m and 8,700 m, respectively, providing clear size thresholds for vegetation and water perimeters. PLAND W and PLAND V displayed a gain–loss relationship, with TVoEs at 2.561% and 97.439%, respectively, indicating the optimal proportion of water and vegetation. Lastly, a TVoE of 1.32 for SHAPE_MN V suggests that vegetation patches with simpler, more square-like shapes are most efficient for maximizing PCA.

https://doi.org/10.5194/isprs-annals-X-5-W4-2025-285-2026 | © Author(s) 2026. CC BY 4.0 License.

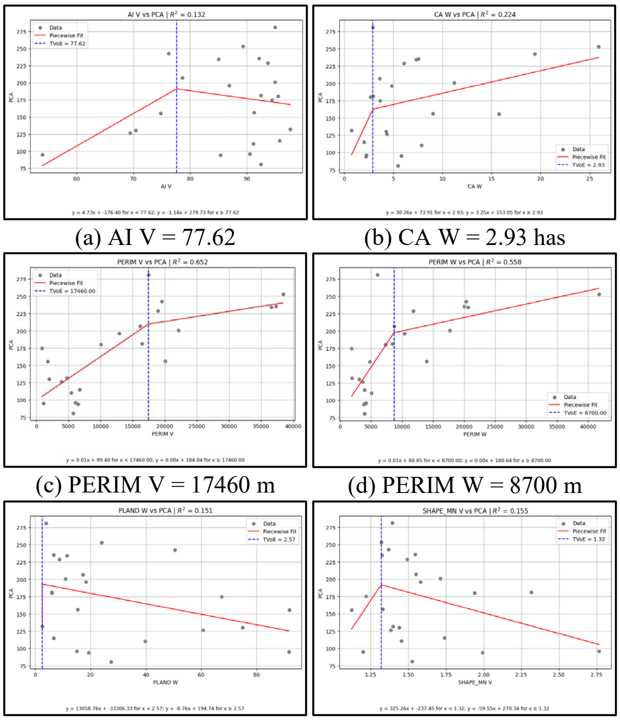

(a) AI V = 77.62 (b) CA W = 2.93 has

(c) PERIM V = 17460 m (d) PERIM W = 8700 m

(e) PLAND W = 2.57% (f) SHAPE_MN V = 1.32

Figure 8. LM – PCA Trend and TVoEs

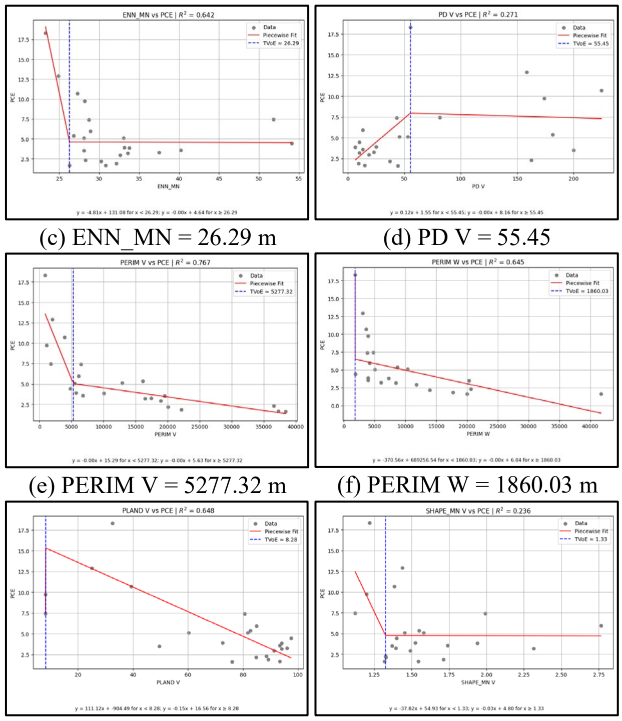

(c) ENN_MN = 26.29 m (d) PD V = 55.45

(e) PERIM V = 5277.32 m (f) PERIM W = 1860.03 m

(g) PLAND V = 8.28% (h) SHAPE_MN V = 1.33

Figure 9. LM– PCE Trend and TVoEs

Figure 9 presents the TVoEs of landscape metrics in relation to PCE, which reflects size-relative cooling effectiveness. CA V showed a downward trend with a TVoE of 14.4 hectares. As a cumulative vegetation area metric, this serves as a tradeoff benchmark. High PCE can be achieved below this threshold, but values beyond 14.4 ha remain viable as the post-TVoE decline is gradual and stable. The same interpretation applies to PERIM V (5,277.32 m) and PERIM W (1,860.03 m), as both are size-related metrics.

ENN_MN and SHAPE_MN V exhibited flat post-TVoE trends, suggesting flexibility. ENN_MN, with a TVoE of 26.29 m, indicates that more aggregated vegetation and water patches are ideal, but PCE remains stable even as distance increases. Similarly, the flat decline beyond the TVoE for SHAPE_MN V implies tolerance for more complex vegetation shapes without significant PCE loss. In contrast, CA W, PD V, and PLAND V demonstrated classical diminishing marginal utility, with TVoEs of 3.65 ha, 55.453, and 8.278%, respectively, indicating that cooling efficiency peaks at these values and diminishes with further increases.

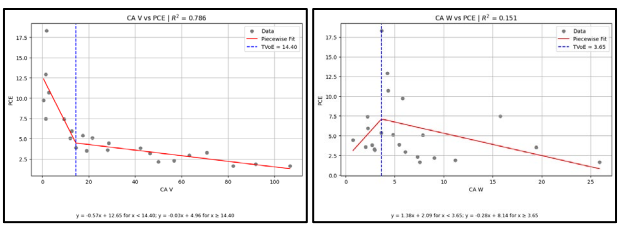

(a) CA V = 14.43 has (b) CA W = 3.65 has

Figure 10 presents the plots and TVoEs of landscape metrics associated with PCG, which captures the spatial gradient of park cooling. CA V showed a tradeoff benchmark with a TVoE of 2.08 hectares, where more intensive cooling occurs below this value. However, exceeding this threshold remains acceptable in multi-metric park designs, as the decline in PCG is minimal. PLAND V and SHAPE_MN V also exhibited negative marginal utility, with TVoEs of 8.70% and 1.219, respectively. The plot for PLAND V suggests that stronger cooling gradients are achieved with a smaller vegetation proportion, favoring water-dominant designs. Still, the nearly flat post-TVoE slope allows for increased vegetation cover with minimal cooling loss, provided other metrics are optimized.

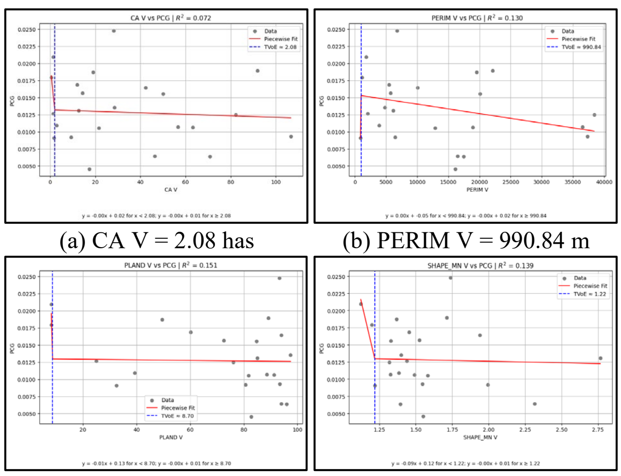

(a) CA V = 2.08 has (b) PERIM V = 990.84 m

(c) PLAND V = 8.70% (d) SHAPE_MN V = 1.22

Figure 10. LM–PCG Trend and TVoEs

Similarly, simpler vegetation shapes are ideal, but SHAPE_MN V's flat post-TVoE slope permits design flexibility. PERIM V demonstrated classical diminishing marginal utility with a TVoE of 990.84 meters. While initial gains are steep, further increases yield progressively smaller improvements in PCG.

Cooling Index	Landscape Metric	Significant TVoE	Interpretation
PCA	CA V (vegetation)	4.12 ha	Larger vegetation patches increase cooling area up to ~4 ha, then level off.
PCA	CA W (water)	2.93 ha	Water patches beyond ~3 ha show diminishing gains in cooling area.
PCA	AI V (vegetation)	77.62	Highly aggregated vegetation boosts PCA until ~78, then plateau.
PCI	CA V (vegetation)	2.08 ha	Intensity rises with vegetation size but stabilizes beyond ~2 ha.
PCI	CA W (water)	3.15 ha	Water helps cooling intensity up to ~3 ha.
PCE	CA V (vegetation)	14.43 ha	Efficiency gains diminish after ~14 ha, showing scale dependence.
PCE	CA W (water)	3.65 ha	Efficiency of water stabilizes beyond ~3.6 ha.
PCE	PLAND V (vegetation)	8.28%	Vegetation proportion beyond ~8% yields diminishing efficiency.
PCG	CA V (vegetation)	2.08 ha	Cooling gradient stabilizes at ~2 ha vegetation patches.
PCG	ENN_MNW (water)	150–200 m	Spatial contrast drives gradients until separation ~200 m.

Table 3. Summary of Significant Landscape Metrics and their TVoEs per Cooling Index in Metro Manila Parks.

3.5.1 Cross-Regional Comparison of TVoEs

The TVoEs derived in this study are broadly consistent with thresholds reported in China and India, though the specific values differ, reflecting the context-dependent nature of park cooling effects emphasized in our introduction.

For vegetation, studies in hot–humid Asian cities such as Dhaka, Kolkata, and Bangkok reported optimal patch sizes ranging from 0.37 to 0.77 has (Fan et al., 2019; Yu et al., 2020). Similar findings were observed in Chinese cities such as Nanjing, where critical patch sizes for vegetation were identified within a comparable range (Sun et al., 2020; Pang et al., 2022). In contrast, our study found thresholds of about 2–14 has, depending on the cooling index. While this confirms the shared principle of diminishing returns across regions, the larger values in Metro Manila suggest that parks must reach greater sizes to offset its denser urban morphology, persistently high background temperatures, and humid tropical climate.

For water bodies, identified patch-size thresholds in Chinese and Indian cities were generally on the order of 1–4 ha, beyond which cooling benefits leveled off. Our findings align with this pattern, with TVoEs of ≈2.9 ha (PCA) and ≈3.6 ha (PCE) for cumulative water area. This convergence suggests that water exerts a relatively stable cooling efficiency across tropical and subtropical settings, though the exact threshold values vary depending on city context, landscape configuration, and analytic method (Peng et al., 2020; Sun et al., 2020; Gupta et al., 2019).

Overall, while Metro Manila's TVoEs echo regional patterns, where small to medium-sized green and blue patches already provide most of the cooling effect, the differences in magnitude highlight the context-specific nature of urban park cooling. Factors such as urban density, climatic conditions, and methodological choices shape the precise thresholds, reinforcing that TVoEs cannot be universally fixed but must be interpreted relative to local urban and environmental contexts.

LM-PCEI	TVoEs in Metro Manila	TVoEs in China / India
CA V – PCE	14.43 ha	0.37–0.77 ha (Fan et al., 2019; Yu et al., 2020)
CA V – PCG	2.08 ha	~0.4–1.0 ha (Sun et al., 2020; Pang et al., 2022)
CA W – PCA	2.93 ha	~1–4 ha (Peng et al., 2020; Sun et al., 2020)
CA W – PCE	3.65 ha	~1–4 ha (Peng et al., 2020; Gupta et al., 2019)
PLAND V – PCE	8.28%	context-dependent thresholds (~5–10%) (Sun et al., 2020)
AI V – PCA	77.62	comparable high aggregation thresholds (Pang et al., 2022)

Table 4. Comparison of TVoEs across Regions.

4. Conclusion

This study revealed that Metro Manila's urban parks exhibit varying cooling effects, with larger parks generally achieving higher cooling areas (PCA), but not necessarily greater cooling intensity (PCI), efficiency (PCE), or gradient (PCG). While park area strongly correlates with PCA ($R = 0.768$), it is less predictive of other indices, which are influenced by spatial contrast, internal configuration, and potentially surrounding land use. Water-related metrics such as PLAND W, AI W, and ENN_MN were found to enhance PCI and PCG, while compact, well-designed parks like Arroceros and San Juan Reservoir demonstrated higher PCE despite their smaller size, highlighting that efficiency can outperform scale.

The relationships between landscape metrics and cooling indices were nonlinear, countering the monotonic expectations of logarithmic models used in prior studies (e.g., Fan et al., 2019; Peng et al., 2020). Piecewise linear regression (PLR) offered the most reliable fit, yielding valid and interpretable TVoEs for 23 landscape metric–cooling index pairs, aligned with diminishing returns logic.

Among the metrics, class area (CA V and CA W) emerged as the most consistent driver, especially for PCA and PCE. However, PCI and PCG showed diminishing returns beyond certain area thresholds, emphasizing that urban park efficiency is not purely scale dependent. Aggregation index (AI V) and shape complexity (SHAPE_MN) also influenced cooling, with aggregated vegetation generally enhancing efficiency. Overall, both compositional (e.g., PLAND, CA) and configurational (e.g., AI, SHAPE_MN, ENN_MN) metrics significantly impact cooling, but their effects are highly nonlinear and context-specific, often diminishing beyond their respective TVoEs.

Nonetheless, several limitations should be considered when interpreting the results. First, the study used a single-date Landsat-8 image from March 6, 2024, which captures peak thermal stress but may not reflect year-round park behaviour. The use of 30-meter resolution data also limited the precision of shape- and edge-sensitive landscape metrics. The supervised classification model, though validated using the 2020 NAMRIA LULC dataset, lacked contemporaneous ground-truthing for 2024, which may have introduced minor inaccuracies. Moreover, vegetation was classified as a single category, potentially obscuring variation in cooling performance across different vegetation types. Lastly, while the TVoE framework effectively captured diminishing returns in most metric–index relationships, its universal applicability may be influenced by local morphology and park context.

These limitations highlight areas for future research, particularly the value of adopting multi-temporal datasets to account for seasonal variation, incorporating higher-resolution spatial imagery to refine metric precision, and disaggregating vegetation classes (e.g., trees, shrubs, and grass) to better capture their differential cooling effects. As such, while the findings provide important insights into the cooling dynamics of Metro Manila's urban parks, they should be interpreted with caution in broader contexts. Validation across multiple cities or temporal scales, along with the incorporation of in-situ ground measurements, would further strengthen the robustness and transferability of the results.

References

Arabi Aliabad, F., Zare, M., Ghafarian Malamiri, H., 2020. A comparative assessment of the accuracies of split-window algorithms for retrieving of land surface temperature using Landsat 8 data. *Modeling Earth Systems and Environment* 7, 2267–2281. doi.org/10.1007/s40808-020-01007-1

Costanza, J.K., Riitters, K., Vogt, P., Wickham, J., 2019. Describing and analyzing landscape patterns: where are we now, and where are we going? *Landscape Ecology* 34, 2049–2055. doi.org/10.1007/s10980-019-00889-6

DOST & PAGASA., 2024. UPDATED COMPUTED AND DAILY HEAT INDEX VALUES. In *https://pubfiles.pagasa.dost.gov.ph*. DOST & PAGASA. https://pubfiles.pagasa.dost.gov.ph/tamss/weather/heat_index_summary.pdf

Fan, H., Yu, Z., Yang, G., Liu, Tsz Yiu, Liu, Tsz Ying, Hung, C.H., Vejre, H., 2019. How to cool hot-humid (Asian) cities with urban trees? An optimal landscape size perspective. *Agricultural and Forest Meteorology* 265, 338–348. doi.org/10.1016/j.agrformet.2018.11.027

Gupta, N., Mathew, A., Khandelwal, S., 2019. Analysis of cooling effect of water bodies on land surface temperature in nearby region: A case study of Ahmedabad and Chandigarh cities in India. *The Egyptian Journal of Remote Sensing and Space Science* 22, 81–93. doi.org/10.1016/j.ejrs.2018.03.007

Hu, Y., Wang, C., Li, J., 2023. Assessment of Heat Mitigation Services Provided by Blue and Green Spaces: An Application of the InVEST Urban Cooling Model with Scenario Analysis in Wuhan, China. *Land* 12, 963. doi.org/10.3390/land12050963

Jimenez-Munoz, J.-C., Sobrino, J.A., 2008. Split-Window Coefficients for Land Surface Temperature Retrieval from Low-Resolution Thermal Infrared Sensors. *IEEE Geoscience and Remote Sensing Letters* 5, 806–809. doi.org/10.1109/LGRS.2008.2001636

Oke, T.R., 1981. Canyon geometry and the nocturnal urban heat island: Comparison of scale model and field observations. *Journal of Climatology* 1, 237–254. doi.org/10.1002/joc.3370010304

Oliveros, J.M., Vallar, E.A., Galvez, M.C.D., 2019. Investigating the Effect of Urbanization on Weather Using the Weather Research and Forecasting (WRF) Model: A Case of Metro Manila, Philippines. *Environments* 6, 10. doi.org/10.3390/environments6020010

Pang, B., Zhao, J., Zhang, J., Yang, L., 2022. How to plan urban green space in cold regions of China to achieve the best cooling efficiency. *Urban Ecosystems* 25, 1181–1198. doi.org/10.1007/s11252-022-01202-1

Peng, J., Liu, Q., Xu, Z., Lyu, D., Du, Y., Qiao, R., Wu, J., 2020. How to effectively mitigate urban heat island effect? A perspective of waterbody patch size threshold. *Landscape and Urban Planning* 202, 103873. doi.org/10.1016/j.landurbplan.2020.103873

Polydoros, A., Cartalis, C., Santamouris, M., Kolokotsa, D., 2022. Chapter 5 - Use of landscape metrics for the mitigation of the surface urban heat island effect in Mediterranean cities, in: Khan, A., Akbari, H., Fiorito, F., Mithun, S., Niyogi, D. (Eds.), Global Urban Heat Island Mitigation. *Elsevier*, pp. 95–108. doi.org/10.1016/B978-0-323-85539-6.00015-9

Sun, X., Tan, X., Chen, K., Song, S., Zhu, X., Hou, D., 2020. Quantifying landscape-metrics impacts on urban green-spaces and water-bodies cooling effect: The study of Nanjing, China. *Urban Forestry & Urban Greening* 55, 126838. doi.org/10.1016/j.ufug.2020.126838

Wu, T., Wang, X., Xuan, L., Yan, Z., Wang, C., Du, C., Su, Y., Duan, J., Yu, K., 2024. How to Plan Urban Parks and the Surrounding Buildings to Maximize the Cooling Effect: A Case Study in Xi'an, China. *Land* 13, 1117. doi.org/10.3390/land13081117

Yan, Z., Wu, T., Xuan, L., Li, W., Wang, X., Dong, L., Yu, K., Wang, Y., 2024. The Scale-Dependent Differences in Cooling Efficiency of UGS in Different Functional Areas: A Case Study of Xi'an, China. *Forests* 15, 1946. doi.org/10.3390/f15111946

Ye, X., Ren, H., Zhu, J., Fan, W., Qin, Q., 2022. Split-Window Algorithm for Land Surface Temperature Retrieval From Landsat-9 Remote Sensing Images. *IEEE Geoscience and Remote Sensing Letters* 19, 1–5. doi.org/10.1109/LGRS.2022.3184980

Yu, Z., Yang, G., Zuo, S., Jørgensen, G., Koga, M., Vejre, H., 2020. Critical review on the cooling effect of urban blue-green space: A threshold-size perspective. *Urban Forestry & Urban Greening* 49, 126630. doi.org/10.1016/j.ufug.2020.126630

Yu, Z., Zhang, J., Yang, G., Schlaberg, J., 2021. Reverse Thinking: A New Method from the Graph Perspective for Evaluating and Mitigating Regional Surface Heat Islands. *Remote Sensing* 13, 1127. doi.org/10.3390/rs13061127

This contribution has been peer-reviewed. The double-blind peer-review was conducted on the basis of the full paper.
https://doi.org/10.5194/isprs-annals-X-5-W4-2025-285-2026